AGU ADVANCING EARTH AND SPACE SCIENCE

Geophysical Research Letters

RESEARCH LETTER
10.1029/2020GL092054

Key Points:

- We obtain conversions between the geometric, aerodynamic, optical, and projected area-equivalent diameters that account for dust asphericity
- Optical particle counters, the sensors most widely used in situ measurements, underestimate dust size at diameters larger than ~8 μm
- Size distributions of emitted dust after harmonizing the different diameter types indicate that models underestimate coarse dust emission

Supporting Information:

- Supporting Information S1

Correspondence to:
Y. Huang,
hyue4@ucla.edu

Citation:
Huang, Y., Adebiyi, A. A., Formenti, P., & Kok, J. F. (2021). Linking the different diameter types of aspherical desert dust indicates that models underestimate coarse dust emission. *Geophysical Research Letters*, *48*, e2020GL092054. https://doi.org/10.1029/2020GL092054

Received 11 DEC 2020
Accepted 5 MAR 2021

Linking the Different Diameter Types of Aspherical Desert Dust Indicates That Models Underestimate Coarse Dust Emission

Yue Huang[1], Adeyemi A. Adebiyi[1], Paola Formenti[2], and Jasper F. Kok[1]

[1]Department of Atmospheric and Oceanic Sciences, University of California, Los Angeles, Los Angeles, CA, USA, [2]Laboratoire Interuniversitaire des Systèmes Atmosphériques, UMR CNRS 7583, Université Paris Est Créteil, Université de Paris, Créteil, France

Abstract Measurements of dust aerosol size usually obtain the optical or projected area-equivalent diameters, whereas model calculations of dust impacts use the geometric or aerodynamic diameters. Accurate conversions between the four diameter types are thus critical. However, most current conversions assume dust is spherical, even though numerous studies show that dust is highly aspherical. Here, we obtain conversions between different diameter types that account for dust asphericity. Our conversions indicate that optical particle counters have underestimated dust geometric diameter (D_{geo}) at coarse sizes. We further use the diameter conversions to obtain a consistent observational constraint on the size distribution of emitted dust. This observational constraint is coarser than parameterizations used in global aerosol models, which underestimate the mass of emitted dust within $10 \leq D_{geo} \leq 20$ μm by a factor of ~2 and usually do not account for the substantial dust emissions with $D_{geo} \geq 20$ μm. Our findings suggest that models substantially underestimate coarse dust emission.

1. Introduction

Desert dust is a key atmospheric component that produces important effects on the Earth system, including by affecting the radiation budget (Kok et al., 2020, 2021; Pérez et al., 2006), cloud microphysics (DeMott et al., 2015), atmospheric chemistry (Tang et al., 2016), and biogeochemical cycles (Ito, Myriokefalitakis, et al., 2019). Furthermore, dust aerosols produce risks to human health (Giannadaki et al., 2014; Huang, Kok, Martin, et al., 2019). These different dust effects are quantified using different types of diameters (Mahowald et al., 2014), but clear links between these different diameter types have not been established. This limits our ability to calculate and understand these various dust impacts, because these impacts depend sensitively on the size of dust aerosols. For example, the radiative effects of fine dust cool the Earth system, whereas coarse dust net warms the planet (Kok, Ridley, et al., 2017).

Four different types of diameters are used in studies of dust and its various impacts (Figure 1a). First, the volume-equivalent diameter (also called the geometric diameter), D_{geo}, is the diameter of a sphere that has the same volume and density as an irregularly shaped dust particle (Hinds, 1999). The geometric diameter can for instance be measured using a Coulter counter, which is a common technique for measuring dust size in ice and marine sediment cores (Delmonte et al., 2002). The geometric diameter is used in global aerosol models to quantify dust size (Mahowald et al., 2014). The size range with $D_{geo} \leq 20$ μm is considered most relevant to dust impacts on weather and climate (Adebiyi & Kok, 2020), although coarser dust can also produce important impacts (Ryder, Highwood, Rosenberg, et al., 2013; Ryder, Highwood, Walser, et al., 2019). Second, the aerodynamic diameter, D_{aero}, is the diameter of a sphere with a density close to water and with the same aerodynamic resistance as a dust particle (Hinds, 1999). The aerodynamic diameter is used in assessing aerosol impacts on human health and in setting air pollution standards (Mahowald et al., 2014). The size ranges with $D_{aero} \leq 2.5$ μm and $D_{aero} \leq 10$ μm (often called $PM_{2.5}$ and PM_{10}) are most relevant to the respiratory risk of dust aerosols and are regulated worldwide (WHO, 2006). Third, the optical diameter, D_{opt}, is the diameter of a calibration particle, generally a polystyrene latex sphere or equivalent non-absorbing material, that produces the same scattered light intensity as the dust particle. The optical diameter is used in optical sizing instruments, such as the optical particle counters (OPCs), the sensors most widely used to measure the particle size distributions (PSDs) of dust aerosols in field campaigns (Formenti et al., 2011).

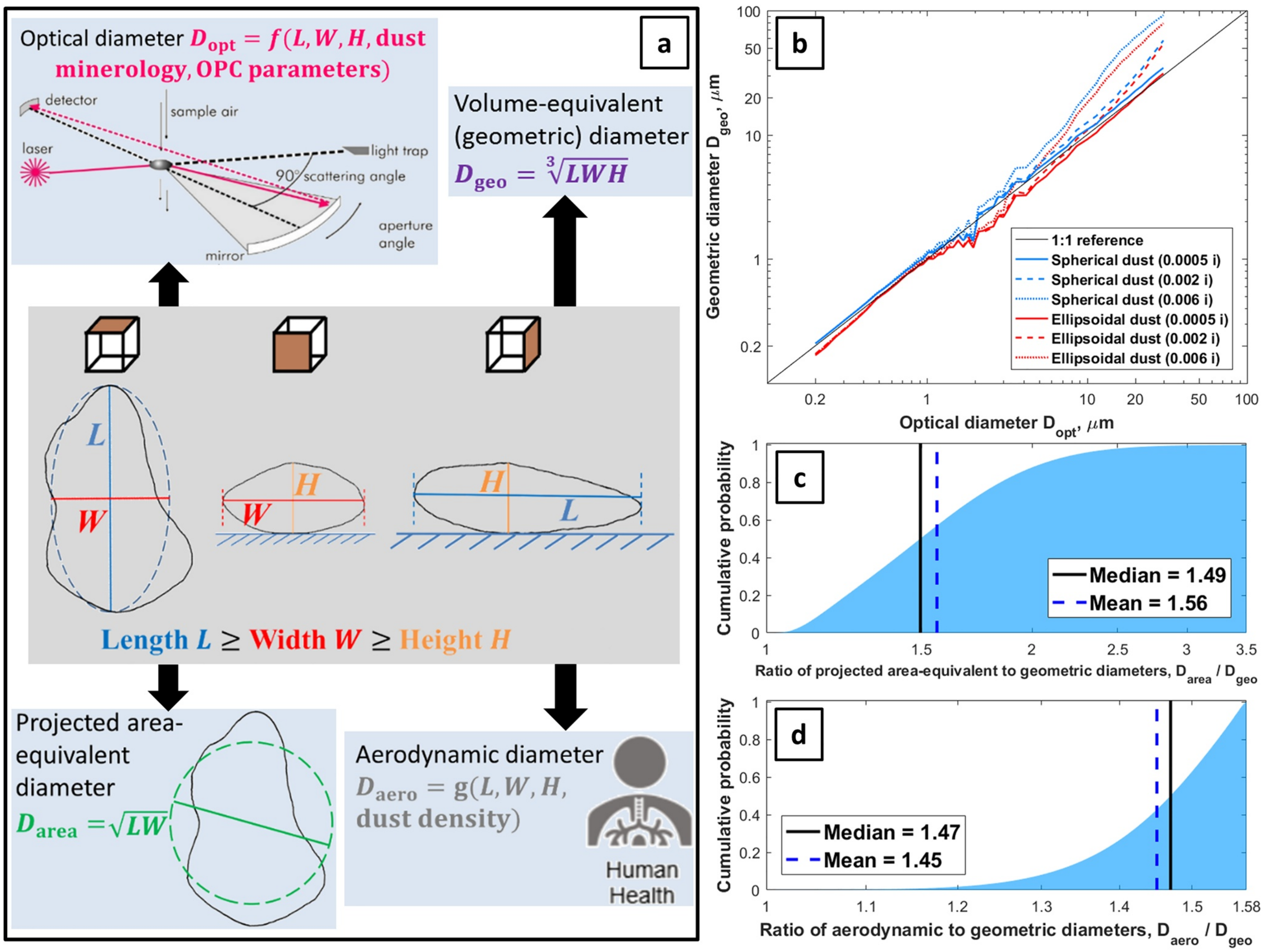

Figure 1. Linking the four different diameter types of aspherical dust. Shown are (a) a schematic of four diameter types of an aspherical dust particle, and conversions between (b) the geometric and optical diameters, (c) the projected area-equivalent and geometric diameters, and (d) the aerodynamic and geometric diameters. Diameter conversions in (b–d) account for dust asphericity using the globally averaged shape distributions (Section 2.1). In (b), the optical particle counter (OPC) wavelength is taken as 780 nm, the scattering angle range is 90° ± 60°, and the real part of dust refractive index is 1.52. Sensitivity tests of the conversion to real and imaginary dust refractive index, wavelength, and scattering angle range are shown in Figures S2–S5, respectively. These results indicate that optical diameter underestimates geometric diameter at coarse sizes, that projected area-equivalent diameter overestimates geometric diameter by 56.3% ± 0.8%, and that aerodynamic diameter exceeds geometric diameter by 44.9% ± 0.3% (standard errors are propagated from errors in globally averaged shape distributions).

The fourth diameter type is the projected area-equivalent diameter, D_{area}, which is the diameter of a circle having the same area as the dust particle projected in a two-dimensional image, usually from scanning electron microscopy (Kandler, Benker, et al., 2007). The projected area-equivalent diameter is used to quantify size-resolved dust mineralogy and morphology (Huang, Kok, Kandler, et al., 2020; Kandler, Lieke, et al., 2011; Swet et al., 2020) and occasionally dust PSDs (Chou et al., 2008; Ryder, Marenco, et al., 2018). These four types of diameters are used for different purposes. In particular, measurements usually determine dust aerosol size in terms of either the optical or projected area-equivalent diameters, whereas model calculations of dust impacts use the geometric or aerodynamic diameters. This makes it critical to reliably link the optical and projected area-equivalent diameters to the geometric and aerodynamic diameters.

Conversions between the four types of diameters generally assume dust is spherical. Specifically, the optical diameter is converted to the geometric diameter using Lorenz-Mie theory (Rosenberg, Dean, et al., 2012), the projected area-equivalent diameter is assumed equal to the geometric diameter (Kandler, Lieke, et al., 2011), and the geometric diameter is converted to the aerodynamic diameter by using the aerodynamic drag law for spherical particles (Hinds, 1999). However, numerous in situ measurements show that dust is highly aspherical (e.g., Kandler, Benker, et al., 2007). Indeed, a recent study that compiled measurements of dust shape worldwide concluded that the ratio of dust's longest to shortest dimensions is ~5 on average (Huang, Kok, Kandler, et al., 2020). Because aspherical dust has substantially different optical, geometric, and aerodynamic properties from spherical dust (Lindqvist et al., 2014; Nousiainen & Kandler, 2015; Yang et al., 2013), diameter conversions that assume a spherical shape are problematic. The resulting biases in size-resolved dust properties can propagate into the calculations of dust impacts on radiative transfer, biogeochemistry, and human health.

To address these problems in converting between different diameter types, here we obtain conversions between four common diameter types that account for dust asphericity (Section 2). In Section 3, we use these diameter conversions to harmonize observational studies that used different types of dust diameters; specifically, we obtain a consistent observational constraint on the size distribution of emitted dust in terms of geometric and aerodynamic diameters. This observational constraint is substantially coarser than parameterizations used in global aerosol models. This finding suggests an underestimation of coarse dust emission by models.

2. Linking the Four Diameters of Aspherical Dust

We first introduce the two shape descriptors that we use to quantify dust asphericity in Section 2.1. By using the two shape descriptors, we approximate dust as tri-axial ellipsoidal particles. We then use the shape-resolved optical, geometric, and aerodynamic properties of ellipsoidal dust to link the four types of diameters in Sections 2.2, 2.3 and 2.4.

2.1. Quantifying Dust Asphericity

We approximate dust as tri-axial ellipsoids whose asphericity is quantified by the ratio of the particle length L to the width W (the aspect ratio, AR) and the height-to-width ratio (HWR) ($L \geq W \geq H$; Figure 1a). Huang, Kok, Kandler, et al. (2020) compiled dozens of measurements of AR$\left(=\frac{L}{W}\right)$ and HWR$\left(=\frac{H}{W}\right)$ worldwide. They found that both AR and HWR deviate substantially from unity, and thus that the ellipsoidal approximation of dust shape is more realistic than spherical or spheroidal approximations. In addition, Huang, Kok, Kandler, et al. (2020) found that both shape descriptors show little dependence on dust size, that AR and HWR are not correlated, and that both HWR and the deviation of AR from unity (AR-1) follow lognormal distributions. Although Huang, Kok, Kandler, et al. (2020) found modest differences in shape distributions for different regions (Table S1), sensitivity tests indicate that these regional differences in dust shape distributions produce only minor differences in diameter conversions (Figure S1). In the present study, we thus take the medians of AR and HWR as 1.70 ± 0.03 and 0.40 ± 0.07, respectively, and the geometric standard deviations of AR-1 and HWR respectively as 0.70 ± 0.02 and 0.73 ± 0.09, after the globally averaged distributions of AR and HWR (Huang, Kok, Kandler, et al., 2020).

2.2. Linking the Optical and Geometric Diameters

The geometric diameter is required in models to calculate dust impacts, whereas most measurements size dust in terms of the optical diameter by using optical particle counters (OPCs) (Formenti et al., 2011). OPCs determine the size and abundance of aerosols by passing a light beam through an aerosol sample and measuring the scattered light intensity by individual aerosol particles (top-left box in Figure 1a). OPC manufacturers calibrate their instruments generally against polystyrene latex spheres (PSLs; ISO, 2009), or occasionally equivalent non-absorbing spheres (Rosenberg, Parker, et al., 2014); by default, OPCs categorize aerosol samples into size bins in terms of the optical diameter of PSLs. This default relationship between measured scattered intensities and optical diameters of spherical PSLs is problematic for particles that are not PSLs, such as dust particles. In this section, we link the optical diameter of spherical PSLs to the geometric diameter of ellipsoidal dust that would generate the same scattered intensity as measured by OPCs.

The scattered intensity produced by an aerosol particle measured by an OPC within the scattering angle range from Θ_1 to Θ_2 (Figure 2f, inset) is (Liou et al., 2002)

$$I_{\mathrm{OPC}} = \frac{I_{\mathrm{i}}}{4\pi} C_{\mathrm{sca}} \int_0^{2\pi} \int_{\Theta_1}^{\Theta_2} P(\Theta) \sin\Theta d\Theta d\phi, \quad (1)$$

where I_{i} (W/m^2) is the incident light intensity that is a constant for a given OPC model, C_{sca} (m^2) is the scattering cross section, $P(\Theta)$ (unitless) is the phase function quantifying the angular distribution of the scattered intensity, and ϕ (sr) is the azimuth angle (Liou et al., 2002). Since most OPCs use a concave mirror to direct and detect scattered light, the scattered intensity measured by most OPCs does not depend on ϕ. For simplicity, we express the normalized scattered intensity measured by OPCs as

$$\mathrm{SI} = \frac{I_{\mathrm{OPC}}}{I_{\mathrm{i}}} = \frac{1}{2} Q_{\mathrm{sca}} A \int_{\Theta_1}^{\Theta_2} P(\Theta) \sin\Theta d\Theta, \quad (2)$$

where $C_{\mathrm{sca}} = Q_{\mathrm{sca}}A$ and Q_{sca} (unitless) is the scattering efficiency that quantifies a particle's ability to scatter relative to its physical cross-sectional area, A (m^2) (Liou et al., 2002). We use Equation 2 to calculate the scattered intensity as a function of the optical diameter of spherical PSLs, and to calculate the scattered intensity of ellipsoidal dust with a wide range of sizes and shape descriptors. For each optical diameter of spherical PSLs, we then determine the average geometric diameter of ellipsoidal dust that produces the same scattered intensity. We discuss these steps in more detail below.

The scattered intensity is sensitive to particle shape. Since PSLs are spherical, we obtained their single-scattering properties, including Q_{sca} and $P(\Theta)$, from Lorenz-Mie theory (Liou, 2002). However, since Lorenz-Mie theory is invalid for aspherical particles, we instead obtained Q_{sca} and $P(\Theta)$ of aspherical dust approximated as ellipsoids by using the single-scattering database of Meng et al. (2010). This database combines four computational methods (Lorenz-Mie theory, T-matrix method, discrete dipole approximation, and an improved geometric optics method) to compute the single-scattering properties of ellipsoidal dust for a wide range of AR, HWR, size parameter, and refractive index. Specifically, we first used Monte-Carlo sampling to randomly generate a large number (10^8) of volume-equivalent ellipsoidal dust from the two lognormal distributions of AR and HWR (Section 2.1). Second, by assuming that each generated particle is randomly oriented, we calculated its A and used the Meng et al. (2010) database to obtain its Q_{sca} and $P(\Theta)$. Finally, we averaged these values and obtained ensemble-averaged values of A, Q_{sca}, and $P(\Theta)$ that account for dust asphericity.

Besides particle shape, the scattered intensity also depends on dust refractive index, the wavelength of the light beam used in the OPC, and the scattering angle range of the OPC's light sensor. OPCs usually measure sideward-scattered intensity within a wide range of scattering angles (e.g., 90° ± 60°) and use visible wavelengths (summarized in Table S2). At these wavelengths, PSLs have a well-calibrated refractive index of $1.59-0i$ (ISO, 2009), whereas the dust refractive index has a large uncertainty (Di Biagio et al., 2017, 2019; Sokolik & Toon, 1999). We used six real parts of dust refractive index between 1.45 and 1.59 and eight imaginary parts between 0.0005 and 0.01 (covering the ranges of Kok, Ridley, et al. [2017] and Di Biagio et al. [2019]). We provided a look-up table that contains the dust refractive index-, wavelength-, and scattering angle range-resolved conversions between the optical diameters of spherical PSLs and the geometric diameters of ellipsoidal dust (Text S1).

We find that OPCs underestimate dust diameter at coarse sizes, due to the combined effects of dust refractive index and dust asphericity. The difference in refractive index between PSLs and dust particles causes the optical diameter to underestimate the size of spherical dust at almost all sizes (blue lines, Figure 1b), but this underestimation due to refractive index difference is offset by dust asphericity (red lines, Figure 1b). We first isolated the effect of dust refractive index by comparing the optical diameter of PSLs with the geometric diameter of spherical dust particles (blue lines, Figure 1b). We find that PSLs produce a larger sideward-scattered intensity than spherical dust particles with the same diameter (black and blue lines, Figure 2a). This occurs because PSLs have a larger real and smaller imaginary refractive index than dust. Thus, a spherical dust with a larger size than a PSL produces the same amount of sideward-scattered intensity as measured by OPCs. Second, we isolated the effect of dust asphericity by comparing the spherical and ellipsoidal dust with the same refractive index (i.e., blue and red dotted lines, Figure 1b). We find that ellipsoidal dust has a larger sideward-scattered intensity than volume-equivalent spherical dust (red and

10.1029/2020GL092054

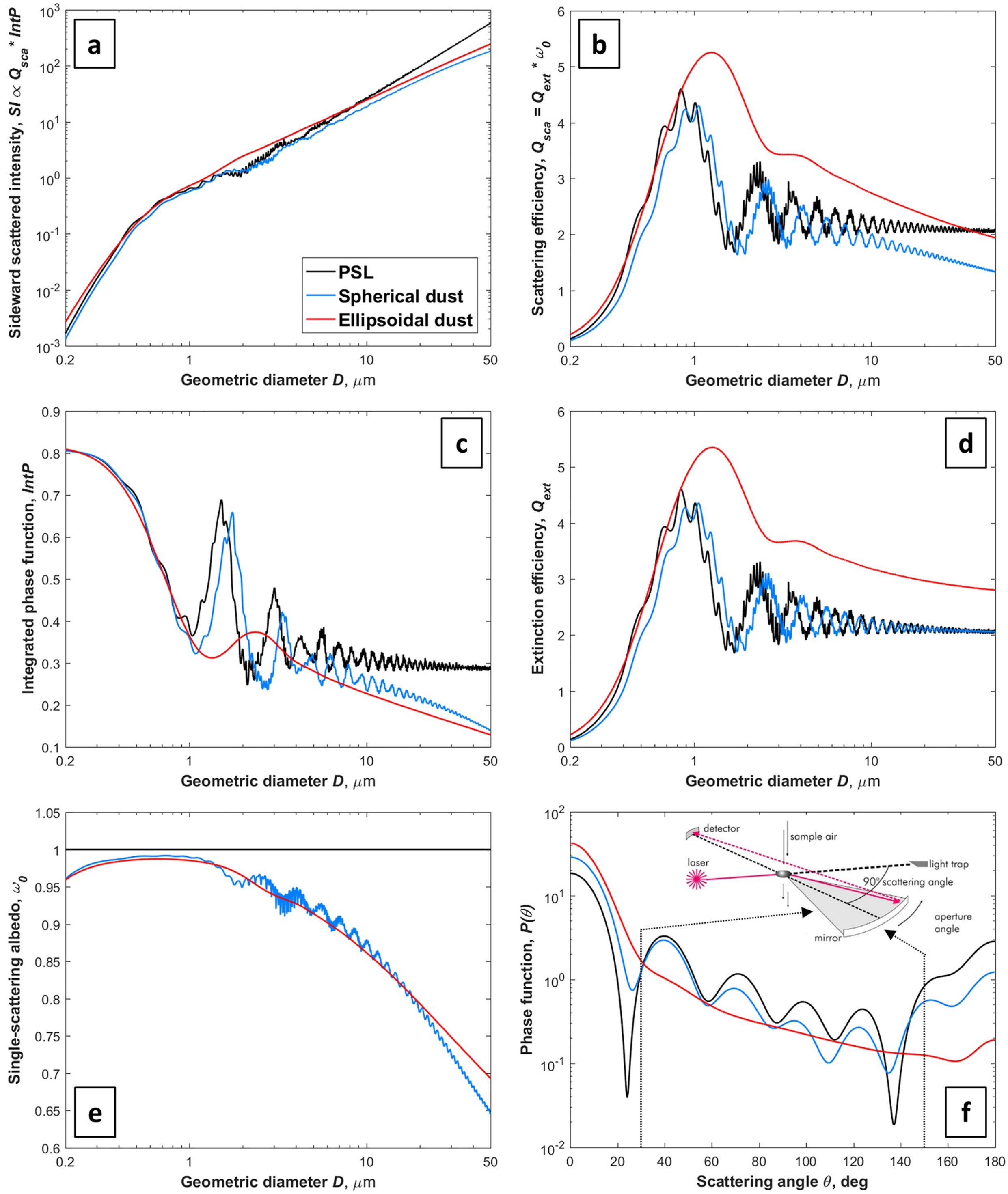

Figure 2. Diagnosis of the factors causing OPCs to underestimate the size of coarse dust. Shown are (a) the sideward-scattered intensity SI, (b) the scattering efficiency Q_{sca}, and (c) the integrated phase function Int$P$, such that SI$\propto Q_{\text{sca}} \times$ Int$P$. The scattering efficiency Q_{sca} is a product of (d) the extinction efficiency Q_{ext} and (e) the single-scattering albedo ω_0. The integrated phase function $\text{Int}P = \frac{1}{2}\int_{\Theta_1}^{\Theta_2} P(\Theta)\sin\Theta d\Theta$ is the (f) phase function $P(\Theta)$ integrated over the scattering angle range measured by OPCs (taken here as 90° ± 60°; range enveloped in black dotted lines in (f)). The inset in (f) shows a schematic of an OPC (GRIMM Model 1.108; permission granted from GRIMM Aerosol Technik Ainring GmbH & Co. KG). Each panel includes results of polystyrene latex spheres (PSLs; black line), spherical dust (blue line), and ellipsoidal dust (red line). Results in each panel are based on a dust refractive index of 1.52–0.002i and a wavelength of 780 nm. In (f), the geometric diameter is 1.5 μm for all three lines.

blue lines, Figure 2a). This occurs because ellipsoidal dust has a larger total scattering efficiency (Figure 2b) but a smaller fraction of that total scattering occurs at angles that OPCs measure (Figure 2c). Thus, the size of an ellipsoidal dust that produces the same amount of sideward-scattered intensity as a PSL is smaller than the size of a spherical dust that produces this intensity (Figure 1b). Finally, after combining the effects of dust refractive index and dust asphericity, we find that OPCs that use optical diameter by default underestimate dust geometric diameter at coarse sizes (red lines, Figure 1b). The diameter at which OPCs start to underestimate dust size decreases substantially with increasing dust imaginary refractive index (red lines, Figure 1b). When the imaginary part increases from 0.0005 to 0.002 and 0.006, the intersection between the red lines and the 1:1 reference line decreases from ∼23 to ∼8, and ∼3 μm in optical diameter. This finding highlights the importance of determining dust imaginary refractive index during in situ measurements to precisely calibrate OPC's size bins and reduce errors in the measured size-resolved data set.

2.3. Linking the Projected Area-Equivalent and Geometric Diameters

After linking the optical and geometric diameters (Section 2.2), we next focus on the projected area-equivalent diameter, which is also commonly used as a measure of dust size (Chou et al., 2008; Gillette, Blifford, & Fenster, 1972). The projected area-equivalent diameter, D_{area}, is obtained from a two-dimensional (2-D) projection image of a 3-D irregularly shaped dust particle with a volume-equivalent diameter of D_{geo} (Figure 1a). Most studies used 2-D optical or scanning electron microscopic images of individual dust particles obtained after these particles were collected on filters by ground-based or aircraft-carried impactors (Gillette, Blifford, & Fenster, 1972; Kandler, Benker, et al., 2007). These impactor-collected dust particles tend to deposit with their largest surface lying parallel to the collection surface, which corresponds to the particle's smallest dimension being oriented perpendicular to the collection surface (Figure 1a). Indeed, Okada et al. (2001) and Sakai et al. (2010) respectively found that about 97% and 95% of dust particles deposited in this manner. Since the smallest dimension (the height H) is on average five times smaller than the largest dimension (the length L) and three times smaller than the intermediate dimension (the width W) (Huang, Kok, Kandler, et al., 2020), the projected area-equivalent diameter substantially overestimates the geometric diameter. To quantify this effect, we assume for simplicity that all dust particles deposit in this orientation, such that the projected area-equivalent diameter equals $D_{\mathrm{area}} = \sqrt{LW}$. We thus express the ratio of the projected area-equivalent and geometric diameters as a function of AR$\left(=\frac{L}{W}\right)$ and HWR$\left(=\frac{H}{W}\right)$ as

$$\frac{D_{\mathrm{area}}}{D_{\mathrm{geo}}} = \frac{\sqrt{LW}}{\sqrt[3]{LWH}} = \frac{\sqrt[6]{AR}}{\sqrt[3]{HWR}}. \tag{3}$$

We used the globally averaged shape distributions of AR and HWR to obtain the probability distribution of $D_{\mathrm{area}}/D_{\mathrm{geo}}$ (Figure 1c). Specifically, we used Monte-Carlo sampling to randomly generate a large number of dust particles from the two lognormal distributions of AR and HWR. Then, for each generated particle, we used Equation 3 to obtain $D_{\mathrm{area}}/D_{\mathrm{geo}}$. We found that the projected area-equivalent diameter is on average 56.3% ± 0.8% larger than the geometric diameter (Figure 1c). This indicates that studies that used projected area-equivalent diameter to quantify dust size have substantially overestimated dust size (e.g., Chou et al., 2008; Gillette, Blifford, & Fenster, 1972).

2.4. Linking the Geometric and Aerodynamic Diameters

After linking the optical, projected area-equivalent, and geometric diameters (Sections 2.2 and 2.3), we next focus on the aerodynamic diameter which is used in assessing dust impacts on human health (Hinds, 1999). The aerodynamic diameter, D_{aero}, is the diameter of a sphere with a density close to water that has the same gravitational settling velocity as the aspherical dust with a geometric diameter of D_{geo} (Hinds, 1999). Gravitational settling of dust aerosols occurs in the Stokes regime as the Reynolds number is far less than one (Kok, Parteli, et al., 2012). In the Stokes regime, the gravitational settling velocity of a spherical particle is (Hinds, 1999)

$$V_{\text{sph}} = \frac{g}{18\mu}\rho D^2, \tag{4}$$

where g is the gravitational acceleration, ρ is the particle density, $\mu \approx 1.81 \times 10^{-5}$ Pa·s is the dynamic viscosity of air, and D is the diameter of the spherical particle. For an aspherical particle, we express its gravitational settling velocity as (Hinds, 1999)

$$V_{\text{asp}} = \frac{1}{\chi}\frac{g}{18\mu}\rho D_{\text{geo}}^2, \tag{5}$$

where χ is the dynamic shape factor that is the ratio of the aerodynamic resistance exerted on an aspherical particle to the resistance on a spherical particle with equal volume and density (Hinds, 1999). By equating the gravitational settling velocities in Equations 4 and 5, we link the aerodynamic and geometric diameters as

$$D_{\text{aero}} = D_{\text{geo}}\sqrt{\frac{\rho_{\text{d}}}{\chi \cdot \rho_0}}, \tag{6}$$

where $\rho_{\text{d}} \approx 2.5 \times 10^3$ kg/m^3 is the typical density of dust aerosols (Kok, Ridley, et al., 2017) and $\rho_0 = 1.0 \times 10^3$ kg/m^3 is the density of water. For aspherical dust approximated as ellipsoids, $\chi = \frac{1}{2}\left(F_{\text{s}}^{1/3} + \frac{1}{F_{\text{s}}^{1/3}}\right)$ and $F_{\text{s}} = HWR \cdot \left(\frac{1}{AR}\right)^{1.3}$ (Bagheri & Bonadonna, 2016; Huang, Kok, Kandler, et al., 2020).

We used the globally averaged shape distributions of AR and HWR to obtain the probability distribution of $D_{\text{aero}}/D_{\text{geo}}$ (Figure 1d). Specifically, we used Monte-Carlo sampling to randomly generate a large number of dust particles from the two lognormal distributions of AR and HWR. Then, for each generated particle, we used Equation 6 to obtain $D_{\text{aero}}/D_{\text{geo}}$. We found that the aerodynamic diameter is on average 44.9% ± 0.3% larger than the geometric diameter (Figure 1d). This result is partially due to dust having a greater density than water, and partially due to dust asphericity increasing the drag force relative to a volume-equivalent sphere.

3. Harmonizing Size Distributions of Emitted Dust

After linking the four diameters of aspherical dust (Section 2), we next use these diameter conversions to harmonize observational studies that sized dust using different diameter types. Eight studies have measured the PSDs of emitted dust in terms of either optical or projected area-equivalent diameters. Three of these studies quantified dust size in terms of projected area-equivalent diameter (Figure 3a; Gillette, 1974; Gillette, Blifford, & Fenster, 1972; Gillette, Blifford, & Fryrear, 1974); they used microscopy to determine the number fluxes of emitted dust from five distinct soils during 29 wind events (summarized in Table S1 of Kok, 2011a). The other five studies used optical diameter (Figure 3a; Fratini et al., 2007; Khalfallah et al., 2020; Rosenberg, Parker, et al., 2014; Shao, Ishizuka, et al., 2011; Sow et al., 2009); they used different OPC models to determine the number fluxes of emitted dust from five distinct regions during 24 wind events (Table S2). Since Gillette (1974) did measurements at three distinct soils, these eight studies yield a total of 10 data sets. These data sets have been used to parameterize the PSD of emitted dust in many modeling studies, thereby implicitly assuming that these different PSDs are in terms of geometric diameter. This includes the study of Kok (2011a), who derived a parameterization of the emitted dust PSD from the analogy of dust emission with the fragmentation of brittle materials such as glass spheres. This "brittle fragmentation theory (BFT)" yielded a relatively simple parameterization that was in good agreement with the (unharmonized) measurements of emitted dust PSDs available at the time. One key prediction of BFT parameterization was that atmospheric dust is substantially coarser than global aerosol models accounted for at the time, which has been supported by a number of subsequent experimental and modeling studies (e.g., Adebiyi & Kok, 2020; Rosenberg, Parker, et al., 2014). The BFT parameterization has been implemented in a large number of global aerosol models (e.g., Klose et al., 2021; Mahowald et al., 2014; Nabat et al., 2012).

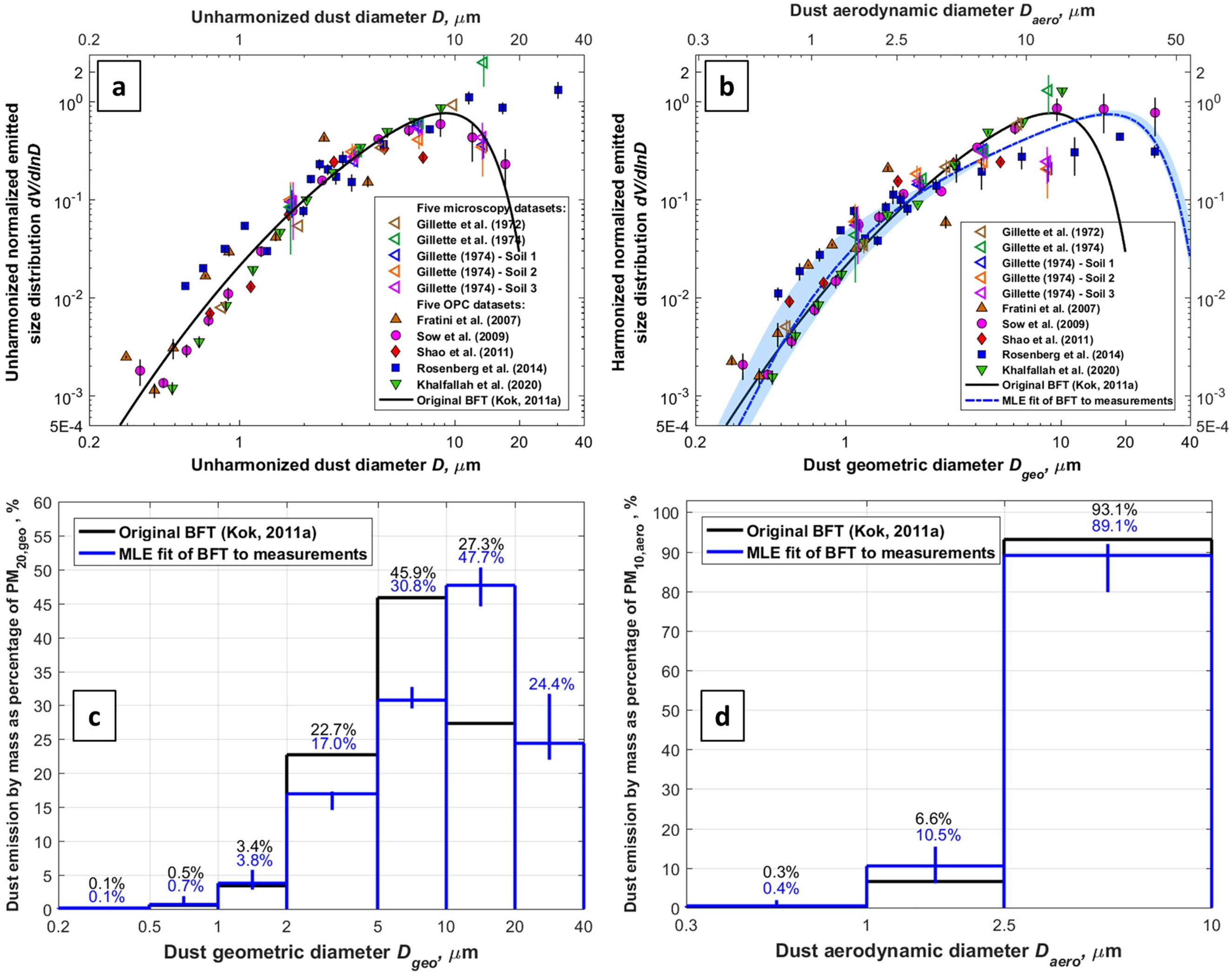

Figure 3. Normalized size distributions of emitted dust (a) before and (b) after harmonizing the different diameter types. Also shown are dust emission flux of individual size bins as percentages of (c) the size range within $0 \le D_{geo} \le 20$ μm ($PM_{20,geo}$) and (d) the size range within $0 \le D_{aero} \le 10$ μm ($PM_{10,aero}$). Vertical error bars in (a and b) denote the standard error of measurements under various wind events at a given soil. In (b), the blue dash-dotted line represents the maximum likelihood estimated (MLE) fit of brittle fragmentation theory (BFT; Kok, 2011a) to the 10 distinct data sets. Blue shading in (b) and vertical error bars in (c and d) denote 95% confidence interval. Compared to the MLE fit, the original BFT parameterization substantially underestimates the mass of emitted dust with $D_{geo} \ge 10$ μm.

We harmonized observational data sets of emitted dust PSDs in order to better inform model parameterizations. We did so by converting the 10 PSDs from either optical or projected area-equivalent diameters to geometric and aerodynamic diameters. First, for the five microscopy data sets, we converted projected area-equivalent diameters to geometric diameters by dividing by the mean of D_{area}/D_{geo} (Figure 1c). For the five OPC data sets, we converted optical diameters to geometric diameters by combining OPC parameters (Table S2) with the look-up table (Text S1). Second, we normalized each PSD data set following Kok (2011a), such that each number PSD of emitted dust follows a power law with exponent of one in the range of $2 \le D_{area} \le 10$ μm (corresponding to $1.28 \le D_{geo} \le 6.41$ μm; Figure 1c). Third, we averaged the volume PSDs of various wind events at a given soil because wind speed has no statistically significant effect on the emitted dust PSD (Kok, 2011b), although a recent study has challenged this finding (Shao, Zhang, et al., 2020). Fourth, we normalized each volume PSD such that its integration over $0 \le D_{geo} \le 20$ μm yields one. Fifth, we obtained the maximum likelihood estimate (MLE) of the harmonized emitted dust PSD following Kok, Ridley, et al. (2017). Specifically, we fit each volume PSD with the analytical function derived from brittle fragmentation theory, and then combined these 10 analytical functions in a statistical model to obtain the

MLE and its 95% confidence interval. Finally, we followed a similar procedure to obtain PSDs in terms of aerodynamic diameter. The above procedure yields a consistent data set of emitted dust PSDs in terms of geometric diameter (bottom *x*-axis, Figure 3b) and aerodynamic diameter (top *x*-axis, Figure 3b).

We obtained two key findings from the harmonized emitted dust PSDs and the MLE fit, which can be taken as the globally representative PSD of emitted dust (see discussion in Kok, Ridley, et al. [2017]). First, the harmonization reduces the divergence in emitted dust PSDs at coarse sizes (from a factor of ∼15 to a factor of ∼2 at diameters larger than ∼12 μm; Figures 3a and 3b). This occurs because, at coarse sizes, OPC studies underestimated geometric diameter (Figure 1b) and thus their PSDs shifted rightward after the harmonization, whereas microscopy studies overestimated geometric diameter (Figure 1c) and thus shifted leftward. The second key finding is that the original BFT parameterization (Kok, 2011a) substantially underestimates the emission of super-coarse dust ($D_{geo} \geq 10$ μm), namely by a factor of ∼2 in the $10 \leq D_{geo} \leq 20$ μm size range (Figure 3c). Furthermore, this parameterization has a cutoff diameter at 20 μm, whereas measurements show a substantial amount of emitted dust with $D_{geo}>20$ μm (Figure 3c). Since the original BFT parameterization is substantially coarser than other parameterizations of the emitted dust PSD (Mahowald et al., 2014), our findings indicate that global aerosol models have substantially underestimated the emission of super-coarse dust.

Our findings have several implications. First, the underestimation of super-coarse dust emission helps explain why models underestimate the concentration of super-coarse dust ($D_{geo} \geq 10$ μm) in the atmosphere. Recent measurements have shown that super-coarse dust is substantially more abundant in the atmosphere than models account for (Adebiyi & Kok, 2020; Glißet al., 2021; Ryder, Marenco, et al., 2018; van der Does, Knippertz, et al., 2018). This model underestimation of super-coarse dust in the air could be due to a number of physical processes omitted or inadequately represented by models, including the slowing of gravitational settling of super-coarse dust by dust asphericity (Huang, Kok, Kandler, et al., 2020), turbulent vertical mixing in dust layers (Gasteiger et al., 2017), electrostatic charging of dust (Harrison et al., 2018), the possible increase in vertical transport of coarse dust by topography-enhanced boundary layer turbulence (Chamecki et al., 2020), and inaccurate representations of wet deposition processes (van der Does, Brummer, et al., 2020; Yu et al., 2019). Our results indicate that models also underestimate super-coarse dust because of a substantial underestimation of super-coarse dust emission.

Second, our results imply a substantial emission (and thus deposition) flux of dust with diameter in excess of 20 μm, which is not accounted for in most models. Our results are consistent with recent measurements finding a substantial amount of dust in the atmosphere with diameters larger than 20 μm (Ryder, Marenco, et al., 2018; van der Does, Knippertz, et al., 2018). However, almost all large-scale models simulate the dust cycle with a cutoff diameter less than 20 μm (Huneeus et al., 2011; Wu et al., 2020). This super-coarse dust produces a net warming (Di Biagio, Balkanski, et al., 2020; Ito, Adebiyi, et al., 2021) and carries more nutrients than fine dust (Marcotte et al., 2020). These important effects of super-coarse dust on weather, climate, and biogeochemistry, especially near source regions, are not accounted for by most models.

Finally, our results suggest that inconsistencies in diameter types used in measurements versus modeling studies have resulted in substantial biases. Studies commonly ignore the difference between diameter types, implicitly assuming that different diameter types are equivalent. We have shown here that this assumption results in substantial errors that propagate into inaccurate estimates of dust impacts. For future studies, we therefore recommend adopting the standardized size conversions obtained here. For published studies, we recommend carefully re-examining, diagnosing, and harmonizing the obtained size-resolved data sets.

4. Conclusions

Measurements of dust aerosol size usually obtain the optical or projected area-equivalent diameters, whereas model calculations of dust impacts use the geometric or aerodynamic diameters. Accurate conversions between the four diameter types are thus critical. However, this critical step of converting between diameter types has been overlooked in many previous studies, for instance in parameterizations of emitted dust size distribution. Furthermore, most existing diameter conversions assume dust is spherical, which is problematic as dust aerosols are highly aspherical.

Here, we address these problems by developing conversions between four diameter types that account for dust asphericity. We found that (1) optical particle counters underestimate dust geometric diameter at $D_{opt} \geq \sim 8$ μm, (2) microscopy measurements using the projected area-equivalent diameter overestimate dust geometric diameter by ∼56%, and (3) the aerodynamic diameter exceeds dust geometric diameter by ∼45%. We encourage the dust research community to use these conversions to more accurately link different diameter types used in observational and modeling studies.

We used these diameter conversions to obtain a consistent observational constraint on the size distribution of emitted dust. This observational constraint is substantially coarser than parameterizations used in global aerosol models, which underestimate the mass of emitted dust within $10 \leq D_{geo} \leq 20$ μm by a factor of ∼2. This finding helps explain why global aerosol models underestimate the abundance of super-coarse dust with $D_{geo} \geq 10$ μm in the atmosphere relative to measurements. Furthermore, our results imply a substantial dust emission and deposition flux with $D_{geo} \geq 20$ μm, which is not accounted for in most models. These models thus neglect the important effects of super-coarse dust on weather, climate, and biogeochemistry, especially near source regions.

Acknowledgments

The authors thank the two anonymous reviewers for their comments that helped to improve the manuscript. Y. Huang acknowledges the financial support by the National Aeronautics and Space Administration (NASA) grant 80NSSC19K1346, awarded under the Future Investigators in NASA Earth and Space Science and Technology (FINESST) program. J. F. Kok acknowledges the support by the National Science Foundation (NSF) grants 1552519 and 1856389, and the Army Research Office under Cooperative Agreement Number W911NF-20-2-0150. A. A. Adebiyi acknowledges the support by University of California President's Postdoctoral Fellowship. P. Formenti acknowledges support by the project DustClim, part of ERA4CS, an ERA-NET initiated by JPI Climate, and funded by FORMAS (SE), DLR (DE), BMWFW (AT), IFD (DK), MINECO (ES), ANR (FR) with co-funding by the European Union (grant 690462). The views and conclusions contained in this manuscript are those of the authors and should not be interpreted as representing the official policies, either expressed or implied, of the Army Research Office or the US Government. The US Government is authorized to reproduce and distribute reprints for Government purposes notwithstanding any copyright notation herein. The authors thank Claudia Di Biagio for providing comments that helped improve the manuscript. In addition, the authors thank Philip Rosenberg and Bouthaina Khalfallah for providing experimental data and thank Carlos Pérez García-Pando, Natalie Mahowald, Konrad Kandler, Yoshihide Takano, Masahide Ishizuka, and Bingqi Yi for insightful discussions. Furthermore, the authors thank Mike Putnam at the Met One Instruments Inc., Randy Grater at the Climet Instruments Co., and Friedhelm Schneider at the GRIMM Aerosol Technik Ainring GmbH & Co. KG for providing information on OPC parameters.

Data Availability Statement

Data sets and code scripts are available in a publicly accessible repository (http://doi.org/10.5281/zenodo.4317642).

References

Adebiyi, A. A., & Kok, J. F. (2020). Climate models miss most of the coarse dust in the atmosphere. *Science Advances*, *6*(15), eaaz9507. https://doi.org/10.1126/sciadv.aaz9507

Bagheri, G., & Bonadonna, C. (2016). On the drag of freely falling non-spherical particles. *Powder Technology*, *301*, 526–544. https://doi.org/10.1016/j.powtec.2016.06.015

Chamecki, M., Freire, L. S., Dias, N. L., Chen, B., Dias-Junior, C. Q., Toledo Machado, L. A., et al. (2020). Effects of vegetation and topography on the boundary layer structure above the Amazon forest. *Journal of the Atmospheric Sciences*, *77*(8), 2941–2957. https://doi.org/10.1175/JAS-D-20-0063.1

Chou, C., Formenti, P., Maille, M., Ausset, P., Helas, G., Harrison, M., & Osborne, S. (2008). Size distribution, shape, and composition of mineral dust aerosols collected during the African Monsoon Multidisciplinary Analysis Special Observation Period 0: Dust and Biomass-Burning Experiment field campaign in Niger, January 2006. *Journal of Geophysical Research*, *113*(23), D00C10. https://doi.org/10.1029/2008JD009897

Delmonte, B., Petit, J., & Maggi, V. (2002). Glacial to Holocene implications of the new 27000-year dust record from the EPICA Dome C (East Antarctica) ice core. *Climate Dynamics*, *18*(8), 647–660. https://doi.org/10.1007/s00382-001-0193-9

DeMott, P. J., Prenni, A. J., McMeeking, G. R., Sullivan, R. C., Petters, M. D., Tobo, Y., et al. (2015). Integrating laboratory and field data to quantify the immersion freezing ice nucleation activity of mineral dust particles. *Atmospheric Chemistry and Physics*, *15*(1), 393–409. https://doi.org/10.5194/acp-15-393-2015

Di Biagio, C., Balkanski, Y., Albani, S., Boucher, O., & Formenti, P. (2020). Direct radiative effect by mineral dust aerosols constrained by new microphysical and spectral optical data. *Geophysical Research Letters*, *47*(2), 1–12. https://doi.org/10.1029/2019GL086186

Di Biagio, C., Formenti, P., Balkanski, Y., Caponi, L., Cazaunau, M., Pangui, E., et al. (2017). Global scale variability of the mineral dust long-wave refractive index: A new dataset of in situ measurements for climate modeling and remote sensing. *Atmospheric Chemistry and Physics*, *17*(3), 1901–1929. https://doi.org/10.5194/acp-17-1901-2017

Di Biagio, C., Formenti, P., Balkanski, Y., Caponi, L., Cazaunau, M., Pangui, E., et al. (2019). Complex refractive indices and single-scattering albedo of global dust aerosols in the shortwave spectrum and relationship to size and iron content. *Atmospheric Chemistry and Physics*, *19*(24), 15503–15531. https://doi.org/10.5194/acp-2019-145

Formenti, P., Schütz, L., Balkanski, Y., Desboeufs, K., Ebert, M., Kandler, K., et al. (2011). Recent progress in understanding physical and chemical properties of African and Asian mineral dust. *Atmospheric Chemistry and Physics*, *11*(16), 8231–8256. https://doi.org/10.5194/acp-11-8231-2011

Fratini, G., Ciccioli, P., Febo, A., Forgione, A., & Valentini, R. (2007). Size-segregated fluxes of mineral dust from a desert area of northern China by eddy covariance. *Atmospheric Chemistry and Physics*, *7*(11), 2133–2168. https://doi.org/10.5194/acpd-7-2133-2007

Gasteiger, J., Groß, S., Sauer, D., Haarig, M., Ansmann, A., & Weinzierl, B. (2017). Particle settling and vertical mixing in the Saharan Air Layer as seen from an integrated model, lidar, and in situ perspective. *Atmospheric Chemistry and Physics*, *17*(1), 297–311. https://doi.org/10.5194/acp-17-297-2017

Giannadaki, D., Pozzer, A., & Lelieveld, J. (2014). Modeled global effects of airborne desert dust on air quality and premature mortality. *Atmospheric Chemistry and Physics*, *14*(2), 957–968. https://doi.org/10.5194/acp-14-957-2014

Gillette, D. A. (1974). On the production of soil wind erosion aerosols having the potential for long range transport. *Journal de Recherches Atmospheriques*, *8*, 734–744.

Gillette, D. A., Blifford, I. H., Jr., & Fenster, C. R. (1972). Measurements of aerosol size distributions and vertical fluxes of aerosols on land subject to wind erosion. *Journal of Applied Meteorology*, *11*(6), 977–987. https://doi.org/10.1175/1520-0450(1972)011<0977:MOASDA>2.0.CO;2

Gillette, D. A., Blifford, I. H., Jr., & Fryrear, D. W. (1974). The influence of wind velocity on the size distributions of aerosols generated by the wind erosion of soils. *Journal of Geophysical Research*, *79*(27), 4068–4075. https://doi.org/10.1029/JC079i027p04068

Gliß, J., Mortier, A., Schulz, M., Andrews, E., Balkanski, Y., Bauer, S. E., et al. (2021). AeroCom phase III multi-model evaluation of the aerosol life cycle and optical properties using ground- and space-based remote sensing as well as surface in situ observations. *Atmospheric Chemistry and Physics*, *21*(1), 87–128. https://doi.org/10.5194/acp-21-87-2021

Harrison, R. G., Nicoll, K. A., Marlton, G. J., Ryder, C. L., & Bennett, A. J. (2018). Saharan dust plume charging observed over the UK. *Environmental Research Letters*, *13*(5), 054018. https://doi.org/10.1088/1748-9326/aabcd9

Hinds, W. C. (1999). *Aerosol technology: Properties, behavior, and measurement of airborne particles* (2nd ed.). Wiley-Interscience.

Huang, Y., Kok, J. F., Kandler, K., Lindqvist, H., Nousiainen, T., Sakai, T., et al. (2020). Climate models and remote sensing retrievals neglect substantial desert dust asphericity. *Geophysical Research Letters*, *47*(6), 1–11. https://doi.org/10.1029/2019GL086592

Huang, Y., Kok, J. F., Martin, R. L., Swet, N., Katra, I., Gill, T. E., et al. (2019). Fine dust emissions from active sands at coastal Oceano Dunes, California. *Atmospheric Chemistry and Physics*, *19*(5), 2947–2964. https://doi.org/10.5194/acp-19-2947-2019

Huneeus, N., Schulz, M., Balkanski, Y., Griesfeller, J., Prospero, J., Kinne, S., et al. (2011). Global dust model intercomparison in AeroCom phase I. *Atmospheric Chemistry and Physics*, *11*(15), 7781–7816. https://doi.org/10.5194/acp-11-7781-2011

ISO (2009). *Determination of particle size distribution: Single particle light interaction methods, part 1: Light scattering aerosol spectrometer*. ISO 21501-1.

Ito, A., Adebiyi, A. A., Huang, Y., & Kok, J. F. (2021). Less atmospheric radiative heating due to aspherical dust with coarser size. *Atmospheric Chemistry and Physics Discussions*. https://doi.org/10.5194/acp-2021-134

Ito, A., Myriokefalitakis, S., Kanakidou, M., Mahowald, N. M., Scanza, R. A., Hamilton, D. S., et al. (2019). Pyrogenic iron: The missing link to high iron solubility in aerosols. *Science Advances*, *5*(5), eaau7671. https://doi.org/10.1126/sciadv.aau7671

Kandler, K., Benker, N., Bundke, U., Cuevas, E., Ebert, M., Knippertz, P., et al. (2007). Chemical composition and complex refractive index of Saharan Mineral Dust at Izaña, Tenerife (Spain) derived by electron microscopy. *Atmospheric Environment*, *41*(37), 8058–8074. https://doi.org/10.1016/j.atmosenv.2007.06.047

Kandler, K., Lieke, K., Benker, N., Emmel, C., Küpper, M., Müller-Ebert, D., et al. (2011). Electron microscopy of particles collected at Praia, Cape Verde, during the Saharan Mineral Dust Experiment: Particle chemistry, shape, mixing state and complex refractive index. *Tellus B: Chemical and Physical Meteorology*, *63*(4), 475–496. https://doi.org/10.1111/j.1600-0889.2011.00550.x

Khalfallah, B., Bouet, C., Labiadh, M. T., Alfaro, S. C., Bergametti, G., Marticorena, B., et al. (2020). Influence of atmospheric stability on the size distribution of the vertical dust flux measured in eroding conditions over a flat bare sandy field. *Journal of Geophysical Research: Atmospheres*, *125*(4), 1–20. https://doi.org/10.1029/2019JD031185

Klose, M., Jorba, O., Gonçalves, M., Escribano, J., Dawson, M. L., Obiso, V., et al. (2021). Mineral dust cycle in the Multiscale Online Nonhydrostatic AtmospheRe CHemistry model (MONARCH) version 2.0. *Geoscientific Model Development Discussions*, 1–59. https://doi.org/10.5194/gmd-2021-32

Kok, J. F. (2011a). A scaling theory for the size distribution of emitted dust aerosols suggests climate models underestimate the size of the global dust cycle. *Proceedings of the National Academy of Sciences*, *108*(3), 1016–1021. https://doi.org/10.1073/pnas.1014798108

Kok, J. F. (2011b). Does the size distribution of mineral dust aerosols depend on the wind speed at emission? *Atmospheric Chemistry and Physics*, *11*(19), 10149–10156. https://doi.org/10.5194/acp-11-10149-2011

Kok, J. F., Adebiyi, A. A., Albani, S., Balkanski, Y., Checa-Garcia, R., Chin, M., et al. (2020). Improved representation of the global dust cycle using observational constraints on dust properties and abundance. *Atmospheric Chemistry and Physics Discussions*, 1–45. https://doi.org/10.5194/acp-2020-1131

Kok, J. F., Adebiyi, A. A., Albani, S., Balkanski, Y., Checa-Garcia, R., Chin, M., et al. (2021). Contribution of the world's main dust source regions to the global cycle of desert dust. *Atmospheric Chemistry and Physics Discussions*, 1–34. https://doi.org/10.5194/acp-2021-4

Kok, J. F., Parteli, E. J. R., Michaels, T. I., & Karam, D. B. (2012). The physics of wind-blown sand and dust. *Reports on Progress in Physics*, *75*(10), 106901. https://doi.org/10.1088/0034-4885/75/10/106901

Kok, J. F., Ridley, D. A., Zhou, Q., Miller, R. L., Zhao, C., Heald, C. L., et al. (2017). Smaller desert dust cooling effect estimated from analysis of dust size and abundance. *Nature Geoscience*, *10*(4), 274–278. https://doi.org/10.1038/ngeo2912

Lindqvist, H., Jokinen, O., Kandler, K., Scheuvens, D., & Nousiainen, T. (2014). Single scattering by realistic, inhomogeneous mineral dust particles with stereogrammetric shapes. *Atmospheric Chemistry and Physics*, *14*(1), 143–157. https://doi.org/10.5194/acp-14-143-2014

Liou, K.-N. (2002). *An introduction to atmospheric radiation* (2nd ed.). Academic Press, Inc.

Mahowald, N., Albani, S., Kok, J. F., Engelstaeder, S., Scanza, R., Ward, D. S., & Flanner, M. G. (2014). The size distribution of desert dust aerosols and its impact on the Earth system. *Aeolian Research*, *15*, 53–71. https://doi.org/10.1016/j.aeolia.2013.09.002

Marcotte, A. R., Anbar, A. D., Majestic, B. J., & Herckes, P. (2020). Mineral dust and iron solubility: Effects of composition, particle size, and surface area. *Atmosphere*, *11*(5), 533–612. https://doi.org/10.3390/atmos11050533

Meng, Z., Yang, P., Kattawar, G. W., Bi, L., Liou, K. N., & Laszlo, I. (2010). Single-scattering properties of tri-axial ellipsoidal mineral dust aerosols: A database for application to radiative transfer calculations. *Journal of Aerosol Science*, *41*(5), 501–512. https://doi.org/10.1016/j.jaerosci.2010.02.008

Nabat, P., Solmon, F., Mallet, M., Kok, J. F., & Somot, S. (2012). Dust emission size distribution impact on aerosol budget and radiative forcing over the Mediterranean region: A regional climate model approach. *Atmospheric Chemistry and Physics*, *12*(21), 10545–10567. https://doi.org/10.5194/acp-12-10545-2012

Nousiainen, T., & Kandler, K. (2015). Light scattering by atmospheric mineral dust particles. *Light Scattering Reviews*, *9*, 3–52. https://doi.org/10.1007/978-3-642-37985-7_1

Okada, K., Heintzenberg, J., Kai, K., & Qin, Y. (2001). Shape of atmospheric mineral particles collected in three Chinese arid-regions. *Geophysical Research Letters*, *28*(16), 3123–3126. https://doi.org/10.1029/2000GL012798

Pérez, C., Nickovic, S., Pejanovic, G., Baldasano, J. M., & Özsoy, E. (2006). Interactive dust-radiation modeling: A step to improve weather forecasts. *Journal of Geophysical Research*, *111*(D16), D16206. https://doi.org/10.1029/2005JD006717

Rosenberg, P. D., Dean, A. R., Williams, P. I., Dorsey, J. R., Minikin, A., Pickering, M. A., & Petzold, A. (2012). Particle sizing calibration with refractive index correction for light scattering optical particle counters and impacts upon PCASP and CDP data collected during the Fennec campaign. *Atmospheric Measurement Techniques*, *5*(5), 1147–1163. https://doi.org/10.5194/amt-5-1147-2012

Rosenberg, P. D., Parker, D. J., Ryder, C. L., Marsham, J. H., Garcia-Carreras, L., Dorsey, J. R., et al. (2014). Quantifying particle size and turbulent scale dependence of dust flux in the Sahara using aircraft measurements. *Journal of Geophysical Research: Atmospheres*, *119*(12), 7577–7598. https://doi.org/10.1002/2013JD021255

Ryder, C. L., Highwood, E. J., Rosenberg, P. D., Trembath, J., Brooke, J. K., Bart, M., et al. (2013). Optical properties of Saharan dust aerosol and contribution from the coarse mode as measured during the Fennec 2011 aircraft campaign. *Atmospheric Chemistry and Physics*, *13*(1), 303–325. https://doi.org/10.5194/acp-13-303-2013

Ryder, C. L., Highwood, E. J., Walser, A., Seibert, P., Philipp, A., & Weinzierl, B. (2019). Coarse and giant particles are ubiquitous in Saharan dust export regions and are radiatively significant over the Sahara. *Atmospheric Chemistry and Physics*, *19*(24), 15353–15376. https://doi.org/10.5194/acp-19-15353-2019

Ryder, C. L., Marenco, F., Brooke, J. K., Estelles, V., Cotton, R., Formenti, P., et al. (2018). Coarse-mode mineral dust size distributions, composition and optical properties from AER-D aircraft measurements over the tropical eastern Atlantic. *Atmospheric Chemistry and Physics*, *18*(23), 17225–17257. https://doi.org/10.5194/acp-18-17225-2018

Sakai, T., Nagai, T., Zaizen, Y., & Mano, Y. (2010). Backscattering linear depolarization ratio measurements of mineral, sea-salt, and ammonium sulfate particles simulated in a laboratory chamber. *Applied Optics*, *49*(23), 4441. https://doi.org/10.1364/AO.49.004441

Shao, Y., Ishizuka, M., Mikami, M., & Leys, J. F. (2011). Parameterization of size-resolved dust emission and validation with measurements. *Journal of Geophysical Research*, *116*(D8), D08203. https://doi.org/10.1029/2010JD014527

Shao, Y., Zhang, J., Ishizuka, M., Mikami, M., Leys, J., & Huang, N. (2020). Dependency of particle size distribution at dust emission on friction velocity and atmospheric boundary-layer stability. *Atmospheric Chemistry and Physics*, *20*(21), 12939–12953. https://doi.org/10.5194/acp-2020-42510.5194/acp-20-12939-2020

Sokolik, I. N., & Toon, O. B. (1999). Incorporation of mineralogical composition into models of the radiative properties of mineral aerosol from UV to IR wavelengths. *Journal of Geophysical Research*, *104*(D8), 9423–9444. https://doi.org/10.1029/1998JD200048

Sow, M., Alfaro, S. C., Rajot, J. L., & Marticorena, B. (2009). Size resolved dust emission fluxes measured in Niger during 3 dust storms of the AMMA experiment. *Atmospheric Chemistry and Physics*, *9*(12), 3881–3891. https://doi.org/10.5194/acp-9-3881-2009

Swet, N., Kok, J. F., Huang, Y., Yizhaq, H., & Katra, I. (2020). Low dust generation potential from active sand grains by wind abrasion. *Journal of Geophysical Research: Earth Surface*, *125*(7), 1–25. https://doi.org/10.1029/2020JF005545

Tang, M., Cziczo, D. J., & Grassian, V. H. (2016). Interactions of water with mineral dust aerosol: Water adsorption, hygroscopicity, cloud condensation, and ice nucleation. *Chemical Reviews*, *116*(7), 4205–4259. https://doi.org/10.1021/acs.chemrev.5b00529

van der Does, M., Brummer, G. J. A., Crimpen, F. C. J., Korte, L. F., Mahowald, N. M., Merkel, U., et al. (2020). Tropical rains controlling deposition of Saharan dust across the North Atlantic Ocean. *Geophysical Research Letters*, *47*(5), 1–10. https://doi.org/10.1029/2019GL086867

van der Does, M., Knippertz, P., Zschenderlein, P., Giles Harrison, R., & Stuut, J.-B. W. (2018). The mysterious long-range transport of giant mineral dust particles. *Science Advances*, *4*(12), eaau2768. https://doi.org/10.1126/sciadv.aau2768

WHO (2006). *WHO air quality guidelines global update 2005: Particulate matter, ozone, nitrogen dioxide and sulfur dioxide. EUR/05/5046029*. Copenhagen: World Health Organization. Retrieved from http://www.euro.who.int/__data/assets/pdf_file/0005/78638/E90038.pdf

Wu, M., Liu, X., Yu, H., Wang, H., Shi, Y., Yang, K., et al. (2020). Understanding processes that control dust spatial distributions with global climate models and satellite observations. *Atmospheric Chemistry and Physics*, *20*(22), 13835–13855. https://doi.org/10.5194/acp-20-13835-2020

Yang, W., Marshak, A., Kostinski, A. B., & Várnai, T. (2013). Shape-induced gravitational sorting of Saharan dust during transatlantic voyage: Evidence from CALIOP lidar depolarization measurements. *Geophysical Research Letters*, *40*(12), 3281–3286. https://doi.org/10.1002/grl.50603

Yu, H., Tan, Q., Chin, M., Remer, L. A., Kahn, R. A., Bian, H., et al. (2019). Estimates of African dust deposition along the trans-Atlantic transit using the decadelong record of aerosol measurements from CALIOP, MODIS, MISR, and IASI. *Journal of Geophysical Research: Atmospheres*, *124*(14), 7975–7996. https://doi.org/10.1029/2019JD030574

References From the Supporting Information

González-Flórez, C., Klose, M., Alastuey, A., Dupont, S., Etyemezian, V., González-Romero, A., et al. (2020). *Understanding size-resolved dust emission from field observations in Morocco*. American Geophysical Union. Fall Meeting 2020, abstract #A041-0005.

Obiso, V., Miller, R. L., Gonçalves, M., Pérez García-Pando, C., & Schuster, G. L. (2020). *Regional variability of dust single scattering albedo due to mineral composition*. American Geophysical Union. Fall Meeting 2020, abstract # A019-04.